Title: Extracellular DNA traps in a ctenophore demonstrate conserved immune cell behaviors in a non-bilaterian

Authors and Affiliations: Lauren E. Vandepas[a,b,c,e*†], Caroline Stefani[c*], Phillip P. Domeier[c], Nikki Traylor-Knowles[d], Frederick W. Goetz[b], William E. Browne[e], Adam Lacy-Hulbert[c]

[a]NRC Research Associateship Program; [b]Northwest Fisheries Science Center, National Oceanographic and Atmospheric Administration, Seattle, WA 98112; [c]Benaroya Research Institute at Virginia Mason, Seattle, WA 98101; [d]University of Miami Rosenstiel School of Marine and Atmospheric Sciences, Miami, FL 33149; [e]University of Miami Department of Biology, Coral Gables, FL 33146; [†]Corresponding author; *Equal contribution

Key Words: Ctenophore; ETosis; immune cell evolution; Mnemiopsis leidyi; Crassostrea gigas; extracellular DNA traps

Subject Areas: Immunology and Inflammation; Evolutionary Biology

Abstract

The formation of extracellular DNA traps (ETosis) is a first response mechanism by specific immune cells following exposure to microbes [1,2]. Initially characterized in vertebrate neutrophils, cells capable of ETosis have been discovered recently in diverse non-vertebrate taxa [3 4-6]. To assess the conservation of ETosis between evolutionarily distant non-vertebrate phyla, we observed and quantified ETosis using the model ctenophore *Mnemiopsis leidyi* and the oyster *Crassostrea gigas*. Here we report that ctenophores – thought to have diverged very early from the metazoan stem lineage [7-10]– possess immune cell types capable of phagocytosis and ETosis. We demonstrate that both *Mnemiopsis* and *Crassostrea* immune cells undergo ETosis after exposure to diverse microbes and chemical agents that stimulate ion flux. Our results support ETosis as an evolutionarily ancient metazoan defense against pathogens.

Main

Response to invading microbes is a primary physiological task for all metazoans. In vertebrates, specialized immune cell types such as macrophages and neutrophils detect the presence of microbes. These immune cells perform specific behaviors like phagocytosis or secretion of antimicrobial compounds to sequester and eliminate microbial invaders [11,12]. The release of extracellular DNA traps (ETs) is a relatively recently described immune cell behavior – a morphologically and molecularly distinct cell death process called ETosis – during which immune cells cast filamentous nets composed of nuclear chromatin material or mitochondrial DNA into the surrounding extracellular space, trapping and killing invading microbes [13,14]. Initially believed to be a behavior exclusive to vertebrate neutrophils, recent studies have highlighted ETosis as an anti-microbial response in non-vertebrate taxa [4,5,15-18]. The independent evolution of ETs has also been proposed in taxa as divergent as social amoebas [19] and plants [20].

In mammalian cells, ETosis and other immune responses are often initiated by pattern recognition receptors (PRRs) that bind to molecular motifs on microbes commonly referred to as pathogen-associated molecular patterns (PAMPs) [21]. PRR protein sequences and domain architectures can vary between taxa, as they evolve to detect host specific pathogens [22-24]. For example, mussels have a radiation of TLRs that may recognize a suite of specific pathogens [25], while *Drosophila* uses its Toll receptors to identify the protein Spätzle [26]. Despite these broad patterns of clade-specific immune receptor diversity, the signaling cascades and effectors downstream of PRRs have been shown to be well conserved [30], including intracellular signaling pathways involving calcium, MAP kinases, and reactive oxygen species (ROS) [27-29].

In vertebrate leukocytes, exposure to cytokines, microbes, PAMPs, or pharmacological agents activate specific cellular pathways involved in ET formation, such as a response to ion imbalance (calcium, potassium) or reactive oxygen species (ROS) burst [31,32]. Although the detailed mechanisms of these pathways remain unknown in non-vertebrates [5,6,14,31,33], genes involved in vertebrate immune cell signaling cascades have been identified in diverse metazoans, including non-bilaterians [34-38].

Non-vertebrate ETosis has been best studied in molluscan model systems, particularly in bivalves like the model oyster *Crassostrea gigas* [4-6,16,39,40]. However, attempts to stimulate production of ETs in *Crassostrea* via exposure to some microbial signatures as well as ETosis-stimulating drugs has yielded variable results [6]. For example, robust ETotic response in oyster hemocytes was observed following challenge with *Vibrio* [4], however induction of ETosis with other microbes or PAMPs has been either modest or not observed [6]. Without a consensus assessment of ETosis stimulation, the conservation of ET induction in non-vertebrates remains unclear, and it is unknown whether ETosis represents a fundamental metazoan immune response [4-6].

Ctenophores, also known as “comb jellies”, are a clade of gelatinous planktonic marine animals that diverged early from the animal stem lineage and represent one of the most ancient extant metazoan phyla [8-10]. Ctenophores have two distinct germ layers (ectoderm and endomesoderm) separated by a jelly-like layer of collagenous mesoglea and lack a circulatory system. Understanding functional attributes of ctenophore physiological systems has provided fundamental insights into the conservation of animal cell types and signaling pathways, as well as revealing mechanisms for the emergence of evolutionary novelties [36,41-43]. Currently, the ctenophore immune system remains almost entirely undescribed [36,44]. Specific immune cell types have not been explicitly identified in ctenophores, though they possess motile amoebocyte-like cells that are abundant in the mesoglea and are capable of phagocytosis [36,45]. Whether ctenophores have additional specialized cellular immune mechanisms has not been reported.

Here we demonstrate that the model ctenophore *Mnemiopsis leidyi* possesses immune cell types capable of ETosis in response to diverse stimuli known to activate conserved signaling cascades in vertebrate immune cells. To rapidly and accurately quantify ETosis we developed a novel, automated imaging pipeline to identify ETs. We applied this imaging pipeline to

comparatively assess ET production in *Mnemiopsis* and the bivalve mollusk *Crassostrea gigas,* a model for invertebrate ETosis. Our data from both non-vertebrate species suggest that cells undergoing ETosis following a range of stimuli represent evolutionarily ancient anti-microbial defense mechanisms in metazoans.

Results

Isolated ctenophore cells display immune behaviors

To investigate whether the model ctenophore *Mnemiopsis leidyi* possesses cell types with specialized immune functions, we mechanically disassociated whole *Mnemiopsis* and examined isolated cells [46,47]. We observed morphologically distinct motile cell types displaying prominent intracellular granules and/or vesicles, including amoebocyte-like cells with relatively short pseudopodia and stellate cells with long pseudopodia (**Fig. 1A-C, Supp. Video 1**). Time-lapse microscopy shows that some stellate cells have a dynamic morphology and can rapidly vary the length and number of pseudopodia (**Supp. Video 2)**. These motile cells are highly active in primary cell cultures and their morphologies and scavenging behaviors are reminiscent of immune cell types, such as macrophage-like cells, that have been described in diverse metazoans [11].

A major role for macrophage-like cells is host defense against microbes. We therefore assessed whether the motile cells present in *Mnemiopsis* exhibited fundamental immune cell behaviors in response to bacteria. *Mnemiopsis* cells were incubated with killed fluorescently labeled *Escherichia coli* and imaged by combined DIC and fluorescence microscopy. We found *Mnemiopsis* cells exhibiting diverse morphologies internalized fluorescent *E. coli* [36]; these included motile stellate and amoeboid cells (**Fig. 1D-F**). Furthermore, timelapse DIC microscopy revealed that amoeboid cells actively maneuvered their pseudopodia to engulf nearby bacteria, supporting a potential role in sensing and removing microbes (**Supp. Video 3**).

Following exposure to *E. coli* a conspicuous subset of stellate cells changed their morphology dramatically by retracting their pseudopodial processes and undergoing nuclear rotation, followed by a rapid expulsion of cellular material (**Fig. 1G; Supp. Video 4; Supp. Video 5**). This behavior is remarkably similar to vertebrate monocyte behavior preceding extracellular DNA trap (ET) formation [31,48]. This led us to speculate that some ctenophore immune cells were producing ETs in response to the presence of microbes.

Ctenophore immune cells produce extracellular traps composed of chromatin

In vertebrates, ETs are released in response to recognition of microbial components, and protect against infection by immobilizing and killing invading microbes[1]. To test whether incubation with microbes promoted extrusion of DNA from *Mnemiopsis* cells we stained isolated cells with Hoechst to label DNA. In isolated cells incubated in seawater media, we observed intact nuclei with concentrated Hoechst labeling (**Fig. 2A**). After treatment with heat-killed fluorescent *E. coli* we observed networks of Hoechst-stained DNA filaments cast in large areas around some individual *Mnemiopsis* cell bodies. Three-dimensional rendering of confocal z-stacks showed that *Mnemiopsis* cells extruding DNA had bacteria entangled in the DNA networks, consistent with ETs (**Fig. 2B; Supp. Video 6;** [49]).

In vertebrate immune cells, ETs can originate either from the cell nucleus or from mitochondria [50,51]. To assess the organellar origin of the extruded DNA, we stained *Mnemiopsis* cells with an antibody that recognizes an array of nuclear histone proteins (H1, H2A, H2B, H3, H4). Nuclei of non-ETotic *Mnemiopsis* cells were labeled with this histone antibody, which showed stereotypical patterns of concentrated DNA and histone labeling, confirming the specificity of this antibody in *Mnemiopsis* cells (**Fig. 2C**) [52,53]. Notably, in cells that have undergone ETosis, the extracellular ET DNA also stained with this pan-histone antibody, demonstrating that the extruded DNA filaments are composed of chromatin (**Fig. 2C, arrows**). Together, these data identify that

Mnemiopsis cells produce *bona fide* extracellular DNA traps and further concluded that these ETs are derived from the nucleus [14].

Ctenophore ETosis is an immune response to microbial exposure

To assess whether the formation of ETs in *Mnemiopsis* is a response to microbial challenge, we measured ET production after incubation of *Mnemiopsis* cells with *E. coli* and two additional microbial particles: heat-killed gram-positive *S. aureus*, and the yeast cell wall extract zymosan. We found that all three microbial particles stimulated ET formation in *Mnemiopsis* cells when compared with untreated cells incubated with media alone (**Fig. 2D**). Numbers of ETotic cells were manually quantified based on release of Hoechst-positive material by fluorescent microscopy (**Fig. 2E**). Exposure to *S. aureus* and zymosan promoted considerably higher rates of ET formation (mean increase of 98.2% and 117.7% over control respectively) than *E. coli* (43.7%) (**Fig. 2E**). These data confirm that production of ETs represents a *Mnemiopsis* immune cell-specific response to the presence of microbes.

Ctenophore ETs form filamentous networks that capture microbes

Scanning electron microscopy (SEM) is commonly used to confirm the structure of ETs, and is informative in distinguishing ETosis from DNA release secondary to other forms of cell death such as necrosis or apoptosis [54]. To examine the structure of the extruded DNA in *Mnemiopsis* cell cultures, we performed SEM on isolated cells that had been incubated with *S. aureus* or with seawater media alone. Images of untreated *Mnemiopsis* cells confirm the presence of diverse morphological cell types observed by DIC, including stellate cells (**Fig. 3A; Supp. Fig. 1).** Following incubation with *S. aureus*, we observed long filamentous networks surrounding some *Mnemiopsis* cells (**Fig. 3B-C; Supp. Fig. 1**), which are similar to ETs produced by vertebrate and crustacean immune cells [1,5,55,56]. We also observed a close association between individual *S. aureus* and the filamentous nets produced by *Mnemiopsis* cells, providing further evidence that these structures are able to capture microbes, a critical function of ETs **(Fig. 3B-C insets**) [57].

PMA induces ETosis in *Mnemiopsis*

We hypothesized that ETosis in ctenophores may be initiated by engaging evolutionarily conserved signaling pathways known to precede ETosis in other metazoans. For example, phorbol 12-myristate 13-acetate (PMA) is commonly used to induce ET production in vertebrate immune cells through activation of NADPH-mediated ROS [31]. This pathway has been proposed to induce ET formation in immune cells in annelids and crustaceans [5,15], suggesting that it may be evolutionarily ancient and well conserved in metazoans. We treated *Mnemiopsis* cells with PMA for four hours, stained DNA with Hoechst, and visualized cells by fluorescence microscopy. We observed the extrusion of DNA after PMA treatment, which was similar ot that seen after micobial challenge (**Fig. 2D; Fig. 4A**).

Importantly, exposure to PMA can also trigger non-ETotic cell death pathways [58], raising the possibility that the extracellular DNA we observed was a result of cell rupture and release of DNA secondary to cell death. To distinguish between these possible scenarios, we used a combination of two DNA dyes: Hoechst, which is a membrane-permeable dye that labels DNA in both live cells and dead cells, and SytoxGreen, a non-permeable cell stain that selectively labels DNA in cells with compromised cell membranes, as observed in cells undergoing cell death (**Fig. 4A**). Both DNA dyes label ETs [5,59], and ETotic cells have both diffuse gradients of Hoechst and Sytox staining (**Fig. 4A-B**). We then developed a semi-automated imaging analysis approach that allowed us to measure Hoescht and SytoxGreen labeling in individual cell nuclei and accurately quantify both ETosis and cell death simultaneously (**Fig. 4B; Supp. Fig. 2**). ET production has been successfully identified and quantified in neutrophils using a combination of machine learning and high-throughput imaging [60,61], we deployed similar techniques to assess ETosis in ctenophore

183 cells. An approach similar to those implemented in flow cytometry analyses was used in which
184 we plotted the intensity of SytoxGreen fluorescence against Hoechst signal for each individual
185 cell (**Fig. 4B-C**). This allowed for the identification of three distinct populations in PMA-treated
186 *Mnemiopsis* cells: Hoechst^{high}/ SytoxGreen^{low} live cells that show no DNA release and intact cell
187 membranes; Hoechst^{low}/ SytoxGreen^{low} cells which display diffuse extracellular Hoechst and
188 SytoxGreen fluorescence, representing ETotic cells [5,59]; and SytoxGreen^{high} cells with a range of
189 Hoescht staining, which are dead or dying non-ETotic cells.
190 To confirm that the image analysis pipeline accurately distinguishes non-ETotic cell death
191 from ETosis, we induced death in *Mnemiopsis* cells by exposure to a moderate osmotic shock
192 (dilute saline solution, 2X PBS). We measured a significant increase in non-ETotic dead cells
193 compared with normal seawater media controls (**Fig. 4C**). Notably, dying cells were clearly
194 separated from cells undergoing ETosis. Using this pipeline, we then quantified ETosis and cell
195 death in cells treated with PMA. Confirming our initial observations by microscopy, PMA promoted
196 significant induction of ETosis, with a mean increase of 57.2% over cells incubated with seawater
197 media alone (**Fig. 4C-D**). Importantly, non-ETotic cell death did not significantly increase following
198 PMA incubation.
199 We sought to establish that the automated image analysis pipeline could detect ETosis
200 induced by microbial exposure. Because we observed clear ETs with SEM following *S. aureus*
201 challenge, we then applied this automated imaging approach to this microbial stimulus. Samples
202 that are incubated with microbes contain more background fluorescence due to Hoescht and
203 Sytox labeling of *S. aureus* nuclear material; however, we observed a clear increase in ETosis
204 following *S. aureus* challenge using automated imaging analysis, as well as an increase in non-
205 ETotic cell death (**Fig. 4C and 4D**). Together, these data confirm that PMA induces ETosis in
206 *Mnemiopsis*. Further, the novel semi-automated image analysis pipeline presented here can
207 accurately detect and quantify invertebrate ETosis and distinguish ETosis from total cell death.
208
209 **ETosis in *Mnemiopsis* is initiated by agonists that induce ion flux**
210 In vertebrates, ET formation can be triggered by membrane ion flux triggered by exposure
211 to bacterial toxins that act as ionophores [31,53,62]. Because stimulation of ETosis via ion flux has
212 limited reports in non-vertebrates [6,32], we assessed whether well-characterized bacterially-derived
213 ionophores nigericin (potassium ionophore) and calcimycin (A23187; calcium ionophore) could
214 also elicit ETosis in *Mnemiopsis* cells. We incubated *Mnemiopsis* cells with the K^+ ionophore
215 nigericin and observed a mean increase of 367% over untreated cells (**Fig. 5A and 5B; Supp.**
216 **Video 6; Supp. Fig. 3**). Incubation with the Ca^{2+} ionophore calcimycin resulted in a mean increase
217 of 225% over untreated control cells (**Fig. 5A and 5B)**. Furthermore, although incubation with
218 either ionophore also significantly increased *Mnemiopsis* cell death, consistent with their effects
219 in vertebrate cells [63-65], our image analysis pipeline was able to clearly distinguish ETosis from
220 other forms of cell death. These data therefore support an evolutionarily conserved pathway for
221 ET formation in response to immune stimulation or cellular damage.
222
223 **Microbes, PMA, and calcium ionophore stimulates ETosis in *Crassostrea gigas* hemocytes**
224 Our observations that ET formation in *Mnemiopsis* can be triggered by similar signaling
225 pathways to those involved in mouse and human immune cell ETosis supports the hypothesis
226 that ETosis represents an evolutionarily ancient response to infection or cell damage activated by
227 intracellular signaling pathways that are widely conserved throughout animals [66-68]. However,
228 stimulation of ETosis has not been widely assessed outside of vertebrates [6,32] or compared
229 between phyla. To compare stimulation of *Mnemiopsis* cells with another non-vertebrate
230 metazoan that is an established model for analysis of ETosis, we extended our analysis to the
231 bivalve mollusc, *Crassostrea gigas*, a marine non-vertebrate bilaterian with a circulatory system
232 possessing specialized immune cells (hemocytes). Some hemocyte cell types have been shown
233 to display immune behaviors such as phagocytosis [69]. We incubated isolated hemocytes with

fluorescent *E. coli* for 4 hours to assess whether *C. gigas* cells were responding to the presence of bacteria by phagocytosing the *E. coli* (**Fig. 6A-B)** or undergoing ETosis (**Fig. 6B,** inset). When observing hemocytes by confocal microscopy, we found that some hemocytes are highly phagocytic, with individual cells ingesting multiple bacteria (**Fig. 6B)**. Fluorescent imaging also identified networks of extracellular DNA surrounding some hemocytes after exposure to microbial particles, similar to previous reports of bivalve ET formation [4] (**Fig. 6B, insets**).

While ETs have been reported in multiple bivalve species, successful induction of ETosis in hemocytes following incubation with either microbial stimuli or pharmaceuticals has varied [4-6]. To directly compare ET production in oyster hemocytes with observations in *Mnemiopsis*, we assessed ETosis in *C. gigas* hemocytes using the same panel of microbes. We first confirmed that *Crassostrea* immune cells undergo ETosis in response to microbial stimulation using the automated imaging analysis pipeline (**Fig. 6C-D**). Hemocytes were incubated with heat-killed *E. coli, S. aureus*, or zymosan, and then assessed using the automated image analysis pipeline for quantification of ETosis. We found that ETosis increased after exposure to all three microbes, when compared to hemocytes incubated *in vitro* with seawater media alone (**Fig 6C-D)**. *Crassostrea* hemocytes undergo ETosis in response to bacterial challenge with both gram-negative *E. coli* and gram-positive *S. aureus* with mean increases of 52.3% and 41.5% over untreated hemocytes, respectively (**Fig. 6D)**. The fungal PAMP zymosan also elicited a significant ETotic response in oyster hemocytes, with a mean increase of 112% over seawater media controls. Interestingly, *S. aureus* stimulation did not stimulate significant increases in non-ETotic cell death in hemocytes (**Fig. 6D**), in contrast to what we observed in *Mnemiopsis* cells (**Fig. 2D-E**). Hemocyte total non-ETotic cell death increased significantly with either *E. coli* or zymosan exposure.

We also measured ETosis in *Crassostrea* hemocytes after four-hour incubations with PMA, nigericin, calcimycin, or seawater media controls (**Fig. 6E-F**). Exposure to PMA induced significant ET production in isolated *Crassostrea* hemocytes, with a relative mean increase of 95.7% (**Fig. 6F**). A large proportion of *Crassostrea* hemocytes also produced ETs after exposure to calcimycin, with a mean increase of 209% over controls (**Fig. 6F**). These results are similar to the robust response reported in prior studies of bivalve hemocytes to Ca^{2+} ionophore stimulation [6]. In contrast to *Mnemiopsis* cells, incubation of hemocytes with the K^+ ionophore nigericin showed no significant induction of ETosis (compare **Fig. 2D-E and Fig. 6F**). Notably, non-ETotic cell death does not increase in *C. gigas* hemocytes following drug incubation. Unexpectedly, both PMA and calcimycin treatment resulted in a relatively minor, but significant, decrease in non-ETotic cell death.

Discussion

Identifying the core molecular mechanisms of immune cells and their evolutionary origins is critical for understanding the evolution of metazoan immune cell function and behavior. Here we report that ctenophores, which diverged very early from the metazoan stem lineage, have immune cells capable of ETosis, a cellular response to microbes first described in mammalinan neutrophils. We also show that cells isolated from the model ctenophore *Mnemiopsis leidyi* undergo ETosis following exposure to diverse microbial components, and stimulation of intracellular signaling cascades known to precede ETosis in vertebrates. For example, we find that incubation with the potassium ionophore nigericin stimulates ETosis in *Mnemiopsis* cells, as has been reported for mammalian neutrophils, suggesting that K^+ efflux may be an evolutionarily conserved trigger for ETosis. We conclude from our results that ETosis represents an ancient mechanism of cellular immune defense in metazoans (**Fig. 7**).

Since the first description of neutrophil extracellular traps [11], multiple pathways involved in the generation of mammalian ETs have been identified [31]. However, the intracellular actors necessary for ET formation in non-vertebrate taxa are less well understood. For example, gene

homologs for proteins known to be essential for ETosis in mammalian neutrophils, such as peptidylarginine deiminase 4 (PAD4), neutrophil elastase, myeloperoxidase (MPO) and pannexin-1 are absent outside of vertebrates. There is strong evidence for the presence of multiple ETosis pathways in non-vertebrates that can be activated via stimulation with microbial signatures, parasites, PMA, A23187, and UV light [4-6,15-17]. Potassium ion efflux, for example, is classically associated with cellular damage, including during bacterial infection [70]. Calcium flux has been implicated in ET formation in vertebrates either as a component of immune receptor-mediated signaling or as an activator of downstream effectors that drive DNA condensation preceding ETosis [71]. In addition to intracellular ion flux, components of vertebrate ETosis pathways, such as ERK, p38, or Akt, are foundational components of metazoan intracellular signaling [66-68].

Our ability to make further direct comparisons of the molecular mechanisms of ETosis between vertebrates and *Mnemiopsis* is currently hampered by a lack of tractable forward genetic approaches and is therefore largely restricted to pharmacological perturbation. However, our data supports considerable apparent conservation of ET formation; firstly, bacterial and fungal components (*E. coli*, intact *S. aureus* and fungal particles) significantly stimulated ETosis in *Mnemiopsis* and *Crassostrea* hemocytes in our study. Our results are in agreement with work in other non-vertebrates and supports the concept that ET formation is a fundamental component of metazoan anti-microbial defense [4-6,15-17]. We also demonstrate that ETosis in *Mnemiopsis* and *Crassostrea* is stimulated by both PMA, which in mammalian cells stimulates protein kinase C and Ca^{2+} flux, and by the Ca^{2+} ionophore A23187. These findings align with observations in vertebrate neutrophils [31] supporting an evolutionarily conserved role for Ca^{2+} transients in ETosis. Finally, the K^{+} ionophore nigericin promoted robust ETosis in *Mnemiopsis*, indicating additional conservation of K^{+} sensing and signaling pathways. Interestingly, *Crassostrea* hemocytes did not produce ETs in response to nigericin, raising the possibility that the nigericin-stimulated pathway is lost in this mollusc species. Signaling pathway inhibitors optimized for use in marine invertebrate cells will be useful for future studies of molecular actors involved in immune responses.

In contrast to vertebrate immune cell nuclear morphologies that correspond with discrete immune cell functions (e.g. lobed nuclei in neutrophils and eosinophils; [72]), no obvious differences in nuclear morphologies have been reported in either bivalve hemocytes or ctenophore immune cells. We did observe that *Mnemiopsis* immune cells that underwent ETosis *in vitro* after exposure to *E. coli* did not appear to have phagocytosed bacteria in significant amounts (**Supp. Video 2**). Intriguingly, we also observed other motile cells that had phagocytosed large amounts of bacteria without undergoing ETosis (**Supp. Fig. 2, Supp. Video 4; Supp. Video 5**). Our functional characterization of ETosis-competent *Mnemiopsis* cells suggests that future studies should assess whether ETosis-competent and highly phagocytic non-ETotic cells represent discrete immune cell types in ctenophores.

Ctenophores have not had specific immune cell antimicrobial behaviors described beyond phagocytosis [36,45]. We demonstrate that *Mnemiopsis leidyi* possesses cells functionally competent for ETosis in response to a range of microbial challenges. It remains unclear whether non-vertebrate immune cells are capable of vital (mitochondrial) ETosis, which involves production of ETs derived from mitochondrial DNA while maintaining cell viability [18]. Our data demonstrates that both *Mnemiopsis leidyi* and *Crassostrea gigas* immune cells can be stimulated to produce ETs with distinct pharmaceutical agents that, in vertebrate immune cells, differentially induce specific intracellular signaling pathways to activate ET production. The production of extracellular traps in *Mnemiopsis* suggests this specific immune cell antimicrobial defense behavior was likely present early in metazoan evolution, prior to the diversification of extant metazoan lineages.

Figure Legends

Figure 1. Stellate and amoebocyte-like *Mnemiopsis* cells display immune behaviors. (A) DIC image of a highly granular amoebocyte-like cell. (B) DIC image of a granular stellate cell displaying multiple processes. (C) DIC image of a stellate cell with pseudopodia. (D) Merged brightfield and fluorescent image of a live *Mnemiopsis* motile, stellate cell that has phagocytosed fluorescent *E. coli* (green). Nuclei are labeled with Hoechst (blue). Lysosomes are labeled with Lysotracker-redDND99 (red). Scale bar is 10 µm. (E)-(F) Combined DIC and fluorescent images of live granular cells with pseudopodia that have phagocytosed fluorescent *E. coli*. (G) Still images from Movie S2 showing a motile stellate cell retracting its processes, undergoing nuclear rotation (spinning), and extruding its nuclear contents after exposure to *E. coli*.

Figure 2. Ctenophore immune cells undergo ETosis when exposed to microbes. (A)-(C) Confocal images of *Mnemiopsis* cell nuclei stained with Hoechst. (A) Left – Nuclei of unstimulated *Mnemiopsis* cells. Right – A cell exposed to fluorescent TxRed-*E. coli* has undergone ETosis; a large web-like pattern of chromatin has been extruded from the cell. Individual *E. coli* can be seen enmeshed by chromatin filaments (white arrowheads). (B) Still images from a 3D projection of *Mnemiopsis* ET. (C) Confocal image of *Mnemiopsis* extracellular traps composed of DNA and histones. Histone 11-4 antibody (green) and Hoechst (white) staining are visible in intact and ETosed *Mnemiopsis* cells treated with the potassium ionophore nigericin. White arrowhead marks extracellular DNA+histone chromatin nets. (D) Fluorescent microscope (Cytation) images of Hoechst-labeled *Mnemiopsis* cells. Representative images of intact nuclei are outlined in white dotted lines, while boundaries of ETs are marked with blue dotted lines. (E) Incubation with *S. aureus*, *E. coli*, and zymosan significantly induced ETosis in *Mnemiopsis* cells. Scale bar is 10 µm in all images.

Figure 3. SEM of *Mnemiopsis* ETs. Scanning electron microscopy (SEM) images of isolated *Mnemiopsis* cells. (A) Images of untreated *Mnemiopsis* stellate cells showing multiple pseudopodial processes. (B)-(C) *Mnemiopsis* cells incubated with *S. aureus* produce extracellular traps composed of long filamentous networks surrounding the cells. Individual *S. aureus* bacterium can be seen closely associated with the filaments. Insets show high magnification of *S. aureus* closely associated with the *Mnemiopsis* ETs. (*S. aureus* are pseudocolored in high magnification for clarity).

Figure 4. PMA stimulation in *Mnemiopsis* evaluated by an automated imaging analysis pipeline. All samples were incubated with their respective stimuli or seawater media alone for 4 hours and imaged. (A) Representative images of untreated controls (top) and PMA-incubated (bottom) *Mnemiopsis* cells labeled with Hoechst and Sytox Green. White dotted lines denote rough boundaries of intact nuclei. Blue dotted lines outline ETs. (B) Representative images of nuclei from SytoxGreen^{high} cells which are dead or dying non-ETotic cells (top), Hoechst^{low}/ SytoxGreen^{low} ETotic cells showing diffuse Hoechst and SytoxGreen fluorescence (middle), Hoechst^{high}/ SytoxGreen^{low} live cells that show intact cell membranes. (C) Representative FlowJo plot showing distribution of fluorescent signals from *Mnemiopsis* cells labeled with Hoechst and SytoxGreen following respective treatments. (D) ETosis is significantly stimulated in *Mnemiopsis* cells are incubated with PMA gram-positive *S. aureus in vitro*. Total cell death increases significantly after incubation with dilute saline compared to seawater control, while detection of ETosis events is unchanged.

Figure 5. ETosis in *Mnemiopsis* is initiated by agonists that induce ion flux. (A) Representative Hoechst-labeled nuclei of untreated controls (left) and cells incubated with either K^+ ionophore nigericin or Ca^{2+} ionophore A23187. White dotted lines denote rough boundaries of intact nuclei. Blue dotted lines outline ETs. (B) Representative FlowJo plot showing distribution of fluorescent signals from cells labeled with Hoechst and SytoxGreen labeled following respective

386 treatments. (C) ETosis is significantly stimulated in *Mnemiopsis* cells incubated with K^+ ionophore
387 nigericin and Ca^{2+} ionophore A23187. Total cell death also increases significantly after incubation
388 with both ionophores.
389
390 **Figure 6. Diverse stimuli induce ETosis in Crassostrea gigas hemocytes.** (A) Confocal image
391 showing *C. gigas* hemocytes that have phagocytosed fluorescent *E. coli*. (B) Confocal image with
392 *C. gigas* hemocytes where some have phagocytosed fluorescent bacteria (arrow) and one cell
393 has produced an ET (arrowhead). Insets show *E. coli* and diffuse DNA staining indicative of
394 ETosis of a hemocyte. (C) (top) Representative images of hemocyte nuclei stained with Hoechst
395 that were either incubated with media alone or exposed to fungal or bacterial PAMPs. White
396 dotted lines denote rough boundaries of intact nuclei. Blue dotted lines outline ETs. (bottom)
397 Representative FlowJo plot showing distribution of fluorescent signals from *C. gigas* hemocytes
398 labeled with Hoechst and SytoxGreen following respective treatments. (D) ETosis is significantly
399 stimulated in *Crassostrea* hemocytes exposed to zymosan, gram-negative *E. coli*, and gram-
400 positive *S. aureus* compared to seawater media controls after 4 hours of incubation. Non-ETotic
401 cell death decreases slightly following zymosan incubation, increases slightly with *E. coli*
402 treatment. No significant change in non-ETotic cell death is detected with *S. aureus* treatment.
403 (E) (top) Representative images of hemocyte nuclei stained with Hoechst that were either
404 incubated with media alone or with PMA, K^+ ionophore nigericin, or Ca^{2+} ionophore A23187. White
405 dotted lines denote rough boundaries of intact nuclei. Blue dotted lines outline ETs. (bottom)
406 Representative FlowJo plot showing distribution of fluorescent signals from *C. gigas* hemocytes
407 labeled with Hoechst and SytoxGreen following respective treatments. (F) PMA and A23187, but
408 not nigericin, significantly stimulate ETosis in hemocytes. Observations of non-ETotic cell death
409 in hemocytes treated with PMA or A23187 decrease.
410 Scale bar is 10 µm in all images.
411
412 **Figure 7. ETosis is an ancient metazoan immune response.** Summary of ETosis phenomena
413 across Metazoa. The presence of cells competent for ETosis in diverse non-bilaterian,
414 protostome, and deuterostome taxa support the production of extracellular DNA traps as an
415 ancient animal immune defense mechanism. Taxa abbreviations: Ch – Choanoflagellata, Ct –
416 Ctenophora, Cn – Cnidaria, Tu – Tunicata, Ve – Vertebrata, An – Annelida, Mo – Mollusca, Cr –
417 Crustacea, He – Hexapoda. Red – this study. Grey – other studies. * – Conflicting reports of
418 ETosis stimulation.
419
420 **<u>Methods</u>**
421
422 *Animal maintenance*
423 Laboratory cultures of *Mnemiopsis leidyi* were maintained as previously described (Presnell, 2021
424 #35). Adult *Mnemiopsis* cells were isolated from whole animals following established protocols
425 [36,46,47]. *Crassostrea gigas* were maintained under flowing seawater at approximately 13°C and
426 hemolymph was extracted from the adductor muscle with a syringe. Isolated cells from both taxa
427 were maintained *in vitro* under sterile conditions in 0.22µm filtered seawater (FSW) + 1%
428 penicillin/streptomycin.
429
430 Scanning electron microscopy (SEM)
431 *Mnemiopsis* cells were seeded onto coverslips treated with poly-L-lysine. Cells were incubated
432 with or without heat-killed *E. coli* for 4 hours to induce ET formation. Cells were fixed in ½ strength
433 Karnovsky's fixative (2.5% glutaraldehyde, 2% paraformaldehyde in 0.1M sodium cacodylate
434 buffer, pH 7.3) overnight at 4°C. Samples were then rinsed with 0.1M cacodylate buffer and
435 treated with 1% osmium tetroxide for 1 hour. The samples were then dehydrated through a graded
436 series of alcohols and critical point dried (Autosamdri, Tousimis Corp, Rockville, MD). Samples

were mounted on stubs, sputter coated with gold/palladium (Denton Desk IV, Denton Vacuum, Moorestown, NJ) and imaged on a JSM 6610 LV scanning electron microscope at 5kV (JEOL, Tokyo, Japan).

Stimulation of ETosis and imaging

For stimulation and quantification of ETosis, cells were isolated from 24 individual animals, plated in 96 well plates, and exposed to pHrodo-*E. coli*, *Staphylococcus aureus*, zymosan particles (Sigma Aldrich), 25 uM nigericin (Thermo Fisher Scientific), 1 mg/mL PMA (Sigma Aldrich), or 4 uM A23187 (Sigma). Each experimental condition for each animal was performed in triplicate. Live cell staining was performed following (2) and live imaging was performed using a JuLI Stage (NanoEntek).

For immunofluorescence, ctenophore cells were prepared as previously described [46,47,73] and labeled with mouse anti-histone H11-4 (EMD Millipore) and anti-mouse Alexa Fluor 488 (Thermo Fisher Scientific). The H11-4 histone antibody was selected because it recognizes histones H1, H2A/B, H3, and H4 proteins across diverse species. Cells were imaged using ×60 objective and ×100 oil objective, on a Nikon Ti (Eclipse) inverted microscope with Ultraview Spinning Disc (CSU-X1) confocal scanner (Perkin Elmer). Images were captured with an Orca-ER Camera using Volocity (Quorum technologies). Post-acquisition analysis such as contrast adjustment, deconvolution through iterative restoration and colocalization were performed using Volocity software.

For quantification of ETosis and total cell death, cells were treated with Hoechst 33342 (Sigma Aldrich) and SytoxGreen (Invitrogen) for 20 min, before imaging at 20X on an automated imaging plate reader, Cytation 3 (Biotek, software Gen5 v4.2).

Automated image-based profiling

We analyzed over 28,000 total images using CellProfiler (v4.1.3). Image quality was assessed by calculating a focus score using two classes Otsu thresholding method, weighted variance on 20x20 pixel measurements. We calculated and applied an illumination correction for each fluorescent channel (SytoxGreen and Hoechst) using a background illumination function of 50 pixels block size, without smoothing. Each corrected image was then segmented using a global robust background method (0.05-50), with a smoothing scale of 1.3488 and a correction factor of 0.89. Clumped objects were identified and split by shape. For each segmented object we measured the number and intensity of pixels in each fluorescent channel. Each image and each segmented object, along with Metadata, were exported as csv files by experiment. R (v4.0.5) software with tidyverse (v1.3.1), dplyr (v1.0.7) and readr (v1.4.0) packages were then used to transform the datasets. Data from images and objects were merged, and measurements from individual images with a Focus Score <0.2 were removed from further analysis. This allowed us to identify and select only images that were in focus. Surface area, Hoechst intensity and SytoxGreen intensity per object (nucleus) and per individual animal were then imported into FlowJo (v10.8.0), and percentages of cells per delineated population (dead/dying cell, live cell, and ETotic cell) were calculated. Dying and ETotic cells were gated as indicated on the figures. Finally, percentages per individual animal surveyed were combined and tested for statistical significance using GraphPad Prism (v9.2.0). All statistical tests were performed using two-tailed unpaired student t-test *$p<0.05$, **$p<0.01$, ***$p<0.001$, ****$p<0.0001$.

Acknowledgements

The authors are grateful to Anna Bruchez and Rachel Prins for imaging support. This research was supported by the National Oceanographic and Atmospheric Administration, a National Research Council Postdoctoral Fellowship to LEV, and the National Science Foundation under Grant No. 2013692. CS and ALH were supported by National Institutes of Health Grants R33AI119341 and R01GM102482. The authors thank Steve Ziegler for technical and

experimental support. The authors gratefully acknowledge the Fred Hutchinson Cancer Center Electron Microscopy Shared Resource (EMSR). The EMSR is supported in part by the Cancer Center Support Grant P30 CA015704-40.

Author contributions

Conceptualization, C.S. and L.E.V.; Methodology, L.E.V. and C.S.; Formal Analysis, C.S. and L.E.V.; Investigation, L.E.V. and C.S.; Visualization, C.S., L.E.V., and W.E.B.; Writing – Original Draft, L.E.V. and C.S.; Writing – Review & Editing, C.S., A.L.H., W.E.B., F.W.G., and L.E.V.; Funding Acquisition, A.L.H., W.E.B., N.T.K., F.W.G., and L.E.V.; Resources, A.L.H., W.E.B., and F.W.G.; Supervision, A.L.H., W.E.B., and F.W.G.

Competing interests

The authors declare no competing interests.

Supplemental Material

Supp. Figure 1: Widefield views of SEM images of unstimulated (left panel) and microbe-challenged (right panel) *Mnemiopsis* cells *in vitro*. Unstimulated cells from whole *Mnemiopsis* show diverse sizes and morphologies indicating the presence of multiple cell types. Microbe-exposed *Mnemiopsis* cells were incubated with *S. aureus* for 3 hours.

Supp. Figure 2: Workflow schematic of the automatic imaging analysis pipeline.

Supp. Video 1: Video of DIC timelapse images of isolated *Mnemiopsis* cells *in vitro*. An amoebocyte-like granular cell (arrowhead) and highly motile stellate cell (arrow) are visible.

Supp. Video 2: Video of DIC timelapse images of an isolated *Mnemiopsis* stellate cell *in vitro*. The cell initially has two large processes, then absorbs them and subsequently produces several additional processes. The cell then begins to crawl out of view.

Supp. Video 3: Merged brightfield and fluorescent video of a live *Mnemiopsis* motile, stellate cell that is phagocytosing fluorescent *E. coli* (green). *Mnemiopsis* cells were labeled with Lysotracker Red. Scale bar is 10 µm.

Supp. Video 4: Merged brightfield and fluorescent video of a live *Mnemiopsis* motile, stellate cell undergoing ETosis after *in vitro* exposure to pHrodo-*E. coli*. The cell moves into view, retracts its processes, spins, and exudes its nuclear material. DNA (Hoechst, blue), pHrodo-*E. coli* (red)

Supp. Video 5: 3D reconstruction of confocal stack of *Mnemiopsis* extracellular DNA traps. DNA (Hoechst, white) is extracellular, in filamentous “nets”; lysosomal marker (Lysotracker, green) denotes cellular debris; bacteria are ensnared in the “nets” (pHrodo-*E. coli*, red)

Supp. Video 6: Merged brightfield and fluorescent video of a live *Mnemiopsis* motile, stellate cell that is phagocytosing fluorescent *E. coli* (red). Scale bar is 10 µm.

REFERENCES:

1 Brinkmann, V. *et al.* Neutrophil extracellular traps kill bacteria. *Science* **303**, 1532-1535 (2004). https://doi.org:10.1126/science.1092385

539 2 Wartha, F., Beiter, K., Normark, S. & Henriques-Normark, B. Neutrophil extracellular traps:
540 casting the NET over pathogenesis. *Curr Opin Microbiol* **10**, 52-56 (2007).
541 https://doi.org:10.1016/j.mib.2006.12.005
542 3 Han, Y., Zhang, Q., Chen, L., Yang, D. & Zhao, J. Mitochondria are essential for
543 antibacterial extracellular trap formation mediated by zymosan in hemocytes of Ruditapes
544 philippinarum. *Dev Comp Immunol* **121**, 104094 (2021).
545 https://doi.org:10.1016/j.dci.2021.104094
546 4 Poirier, A. C. *et al.* Antimicrobial histones and DNA traps in invertebrate immunity:
547 evidences in Crassostrea gigas. *J Biol Chem* **289**, 24821-24831 (2014).
548 https://doi.org:10.1074/jbc.M114.576546
549 5 Robb, C. T., Dyrynda, E. A., Gray, R. D., Rossi, A. G. & Smith, V. J. Invertebrate
550 extracellular phagocyte traps show that chromatin is an ancient defence weapon. *Nat*
551 *Commun* **5**, 4627 (2014). https://doi.org:10.1038/ncomms5627
552 6 Romero, A., Novoa, B. & Figueras, A. Extracellular traps (ETosis) can be activated through
553 NADPH-dependent and -independent mechanisms in bivalve mollusks. *Dev Comp*
554 *Immunol* **106**, 103585 (2020). https://doi.org:10.1016/j.dci.2019.103585
555 7 Dunn, C. W. *et al.* Broad phylogenomic sampling improves resolution of the animal tree of
556 life. *Nature* **452**, 745-749 (2008). https://doi.org:10.1038/nature06614
557 8 Li, Y., Shen, X. X., Evans, B., Dunn, C. W. & Rokas, A. Rooting the Animal Tree of Life.
558 *Mol Biol Evol* **38**, 4322-4333 (2021). https://doi.org:10.1093/molbev/msab170
559 9 Redmond, A. K. & McLysaght, A. Evidence for sponges as sister to all other animals from
560 partitioned phylogenomics with mixture models and recoding. *Nat Commun* **12**, 1783
561 (2021). https://doi.org:10.1038/s41467-021-22074-7
562 10 Schultz, D. T. *et al.* Ancient gene linkages support ctenophores as sister to other animals.
563 *Nature* **618**, 110-117 (2023). https://doi.org:10.1038/s41586-023-05936-6
564 11 Buchmann, K. Evolution of Innate Immunity: Clues from Invertebrates via Fish to
565 Mammals. *Front Immunol* **5**, 459 (2014). https://doi.org:10.3389/fimmu.2014.00459
566 12 Mandujano-Tinoco, E. A., Sultan, E., Ottolenghi, A., Gershoni-Yahalom, O. & Rosental, B.
567 Evolution of Cellular Immunity Effector Cells; Perspective on Cytotoxic and Phagocytic
568 Cellular Lineages. *Cells* **10** (2021). https://doi.org:10.3390/cells10081853
569 13 Fuchs, T. A. *et al.* Novel cell death program leads to neutrophil extracellular traps. *J Cell*
570 *Biol* **176**, 231-241 (2007). https://doi.org:10.1083/jcb.200606027
571 14 Sollberger, G., Tilley, D. O. & Zychlinsky, A. Neutrophil Extracellular Traps: The Biology
572 of Chromatin Externalization. *Dev Cell* **44**, 542-553 (2018).
573 https://doi.org:10.1016/j.devcel.2018.01.019
574 15 Homa, J., Ortmann, W. & Kolaczkowska, E. Conservative Mechanisms of Extracellular
575 Trap Formation by Annelida Eisenia andrei: Serine Protease Activity Requirement. *PLoS*
576 *One* **11**, e0159031 (2016). https://doi.org:10.1371/journal.pone.0159031
577 16 Lange, M. K. *et al.* Gastropod-derived haemocyte extracellular traps entrap
578 metastrongyloid larval stages of Angiostrongylus vasorum, Aelurostrongylus abstrusus
579 and Troglostrongylus brevior. *Parasit Vectors* **10**, 50 (2017).
580 https://doi.org:10.1186/s13071-016-1961-z
581 17 Nascimento, M. T. C. *et al.* DNA extracellular traps are part of the immune repertoire of
582 Periplaneta americana. *Dev Comp Immunol* **84**, 62-70 (2018).
583 https://doi.org:10.1016/j.dci.2018.01.012
584 18 Ramos-Martinez, E. *et al.* Multiple Origins of Extracellular DNA Traps. *Front Immunol* **12**,
585 621311 (2021). https://doi.org:10.3389/fimmu.2021.621311
586 19 Zhang, X., Zhuchenko, O., Kuspa, A. & Soldati, T. Social amoebae trap and kill bacteria
587 by casting DNA nets. *Nat Commun* **7**, 10938 (2016).
588 https://doi.org:10.1038/ncomms10938

589 20 Wen, F., White, G. J., VanEtten, H. D., Xiong, Z. & Hawes, M. C. Extracellular DNA is
590 required for root tip resistance to fungal infection. *Plant Physiol* **151**, 820-829 (2009).
591 https://doi.org:10.1104/pp.109.142067
592 21 Ward, J. R. *et al.* A central role for monocytes in Toll-like receptor-mediated activation of
593 the vasculature. *Immunology* **128**, 58-68 (2009). https://doi.org:10.1111/j.1365-
594 2567.2009.03071.x
595 22 Zhang, Q., Zmasek, C. M. & Godzik, A. Domain architecture evolution of pattern-
596 recognition receptors. *Immunogenetics* **62**, 263-272 (2010).
597 https://doi.org:10.1007/s00251-010-0428-1
598 23 Snoeck, S. *et al.* Evolutionary gain and loss of a plant pattern-recognition receptor for
599 HAMP recognition. *Elife* **11** (2022). https://doi.org:10.7554/eLife.81050
600 24 Tassia, M. G., Whelan, N. V. & Halanych, K. M. Toll-like receptor pathway evolution in
601 deuterostomes. *Proc Natl Acad Sci U S A* **114**, 7055-7060 (2017).
602 https://doi.org:10.1073/pnas.1617722114
603 25 Saco, A., Novoa, B., Greco, S., Gerdol, M. & Figueras, A. Bivalves Present the Largest
604 and Most Diversified Repertoire of Toll-Like Receptors in the Animal Kingdom, Suggesting
605 Broad-Spectrum Pathogen Recognition in Marine Waters. *Mol Biol Evol* **40** (2023).
606 https://doi.org:10.1093/molbev/msad133
607 26 Parthier, C. *et al.* Structure of the Toll-Spatzle complex, a molecular hub in Drosophila
608 development and innate immunity. *Proc Natl Acad Sci U S A* **111**, 6281-6286 (2014).
609 https://doi.org:10.1073/pnas.1320678111
610 27 Dong, C., Davis, R. J. & Flavell, R. A. MAP kinases in the immune response. *Annu Rev*
611 *Immunol* **20**, 55-72 (2002). https://doi.org:10.1146/annurev.immunol.20.091301.131133
612 28 Gostner, J. M., Becker, K., Fuchs, D. & Sucher, R. Redox regulation of the immune
613 response. *Redox Rep* **18**, 88-94 (2013).
614 https://doi.org:10.1179/1351000213Y.0000000044
615 29 Vig, M. & Kinet, J. P. Calcium signaling in immune cells. *Nat Immunol* **10**, 21-27 (2009).
616 https://doi.org:10.1038/ni.f.220
617 30 Akira, S., Uematsu, S. & Takeuchi, O. Pathogen recognition and innate immunity. *Cell*
618 **124**, 783-801 (2006). https://doi.org:10.1016/j.cell.2006.02.015
619 31 Kenny, E. F. *et al.* Diverse stimuli engage different neutrophil extracellular trap pathways.
620 *Elife* **6** (2017). https://doi.org:10.7554/eLife.24437
621 32 Auguste, M., Balbi, T., Ciacci, C. & Canesi, L. Conservation of Cell Communication
622 Systems in Invertebrate Host-Defence Mechanisms: Possible Role in Immunity and
623 Disease. *Biology (Basel)* **9** (2020). https://doi.org:10.3390/biology9080234
624 33 Douda, D. N., Khan, M. A., Grasemann, H. & Palaniyar, N. SK3 channel and mitochondrial
625 ROS mediate NADPH oxidase-independent NETosis induced by calcium influx. *Proc Natl*
626 *Acad Sci U S A* **112**, 2817-2822 (2015). https://doi.org:10.1073/pnas.1414055112
627 34 Ryan, J. F. *et al.* The genome of the ctenophore Mnemiopsis leidyi and its implications for
628 cell type evolution. *Science* **342**, 1242592 (2013).
629 https://doi.org:10.1126/science.1242592
630 35 Moroz, L. L. *et al.* The ctenophore genome and the evolutionary origins of neural systems.
631 *Nature* **510**, 109-114 (2014). https://doi.org:10.1038/nature13400
632 36 Traylor-Knowles, N., Vandepas, L. E. & Browne, W. E. Still Enigmatic: Innate Immunity in
633 the Ctenophore Mnemiopsis leidyi. *Integr Comp Biol* **59**, 811-818 (2019).
634 https://doi.org:10.1093/icb/icz116
635 37 Srivastava, M. *et al.* The Amphimedon queenslandica genome and the evolution of animal
636 complexity. *Nature* **466**, 720-726 (2010). https://doi.org:10.1038/nature09201
637 38 Putnam, N. H. *et al.* Sea anemone genome reveals ancestral eumetazoan gene repertoire
638 and genomic organization. *Science* **317**, 86-94 (2007).
639 https://doi.org:10.1126/science.1139158

39 Bachere, E. *et al.* The new insights into the oyster antimicrobial defense: Cellular, molecular and genetic view. *Fish Shellfish Immunol* **46**, 50-64 (2015). https://doi.org:10.1016/j.fsi.2015.02.040

40 Jiang, S. *et al.* Functional characterisation of phagocytes in the Pacific oyster Crassostrea gigas. *PeerJ* **4**, e2590 (2016). https://doi.org:10.7717/peerj.2590

41 Babonis, L. S., Ryan, J. F., Enjolras, C. & Martindale, M. Q. Genomic analysis of the tryptome reveals molecular mechanisms of gland cell evolution. *Evodevo* **10**, 23 (2019). https://doi.org:10.1186/s13227-019-0138-1

42 Jokura, K. *et al.* CTENO64 Is Required for Coordinated Paddling of Ciliary Comb Plate in Ctenophores. *Curr Biol* **29**, 3510-3516 e3514 (2019). https://doi.org:10.1016/j.cub.2019.08.059

43 Presnell, J. S. & Browne, W. E. Kruppel-like factor gene function in the ctenophore Mnemiopsis leidyi assessed by CRISPR/Cas9-mediated genome editing. *Development* **148** (2021). https://doi.org:10.1242/dev.199771

44 Bolte, S. *et al.* Specific immune priming in the invasive ctenophore Mnemiopsis leidyi. *Biol Lett* **9**, 20130864 (2013). https://doi.org:10.1098/rsbl.2013.0864

45 Franc, J. M. La matrice mésogléenne des Cténaires. *Bulletin de la Société zoologique de France* **113**, 347-447 (1988).

46 Dieter, A. C., Vandepas, L. E. & Browne, W. E. Isolation and Maintenance of In Vitro Cell Cultures from the Ctenophore Mnemiopsis leidyi. *Methods Mol Biol* **2450**, 347-358 (2022). https://doi.org:10.1007/978-1-0716-2172-1_18

47 Vandepas, L. E., Warren, K. J., Amemiya, C. T. & Browne, W. E. Establishing and maintaining primary cell cultures derived from the ctenophore Mnemiopsis leidyi. *J Exp Biol* **220**, 1197-1201 (2017). https://doi.org:10.1242/jeb.152371

48 Boe, D. M., Curtis, B. J., Chen, M. M., Ippolito, J. A. & Kovacs, E. J. Extracellular traps and macrophages: new roles for the versatile phagocyte. *J Leukoc Biol* **97**, 1023-1035 (2015). https://doi.org:10.1189/jlb.4RI1014-521R

49 Apel, F. *et al.* The cytosolic DNA sensor cGAS recognizes neutrophil extracellular traps. *Sci Signal* **14** (2021). https://doi.org:10.1126/scisignal.aax7942

50 Yousefi, S. *et al.* Catapult-like release of mitochondrial DNA by eosinophils contributes to antibacterial defense. *Nat Med* **14**, 949-953 (2008). https://doi.org:10.1038/nm.1855

51 Lood, C. *et al.* Neutrophil extracellular traps enriched in oxidized mitochondrial DNA are interferogenic and contribute to lupus-like disease. *Nat Med* **22**, 146-153 (2016). https://doi.org:10.1038/nm.4027

52 Nagase, H., Ueki, S. & Fujieda, S. The roles of IL-5 and anti-IL-5 treatment in eosinophilic diseases: Asthma, eosinophilic granulomatosis with polyangiitis, and eosinophilic chronic rhinosinusitis. *Allergol Int* **69**, 178-186 (2020). https://doi.org:10.1016/j.alit.2020.02.002

53 Fukuchi, M. *et al.* How to detect eosinophil ETosis (EETosis) and extracellular traps. *Allergol Int* **70**, 19-29 (2021). https://doi.org:10.1016/j.alit.2020.10.002

54 de Buhr, N. & von Kockritz-Blickwede, M. How Neutrophil Extracellular Traps Become Visible. *J Immunol Res* **2016**, 4604713 (2016). https://doi.org:10.1155/2016/4604713

55 Barnes, B. J. *et al.* Targeting potential drivers of COVID-19: Neutrophil extracellular traps. *J Exp Med* **217** (2020). https://doi.org:10.1084/jem.20200652

56 Zhao, M. L., Chi, H. & Sun, L. Neutrophil Extracellular Traps of Cynoglossus semilaevis: Production Characteristics and Antibacterial Effect. *Front Immunol* **8**, 290 (2017). https://doi.org:10.3389/fimmu.2017.00290

57 Brinkmann, V. & Zychlinsky, A. Neutrophil extracellular traps: is immunity the second function of chromatin? *J Cell Biol* **198**, 773-783 (2012). https://doi.org:10.1083/jcb.201203170

58 Seo, K. S. *et al.* PMA synergistically enhances apicularen A-induced cytotoxicity by disrupting microtubule networks in HeLa cells. *BMC Cancer* **14**, 36 (2014). https://doi.org:10.1186/1471-2407-14-36

59 Riegger, J. *et al.* Histopathological evaluation of thrombus in patients presenting with stent thrombosis. A multicenter European study: a report of the prevention of late stent thrombosis by an interdisciplinary global European effort consortium. *Eur Heart J* **37**, 1538-1549 (2016). https://doi.org:10.1093/eurheartj/ehv419

60 Elsherif, L. *et al.* Machine Learning to Quantitate Neutrophil NETosis. *Sci Rep* **9**, 16891 (2019). https://doi.org:10.1038/s41598-019-53202-5

61 Gupta, S., Chan, D. W., Zaal, K. J. & Kaplan, M. J. A High-Throughput Real-Time Imaging Technique To Quantify NETosis and Distinguish Mechanisms of Cell Death in Human Neutrophils. *J Immunol* **200**, 869-879 (2018). https://doi.org:10.4049/jimmunol.1700905

62 Remijsen, Q. *et al.* Dying for a cause: NETosis, mechanisms behind an antimicrobial cell death modality. *Cell Death Differ* **18**, 581-588 (2011). https://doi.org:10.1038/cdd.2011.1

63 Ojcius, D. M., Zychlinsky, A., Zheng, L. M. & Young, J. D. Ionophore-induced apoptosis: role of DNA fragmentation and calcium fluxes. *Exp Cell Res* **197**, 43-49 (1991). https://doi.org:10.1016/0014-4827(91)90477-c

64 Yu, S. P. Regulation and critical role of potassium homeostasis in apoptosis. *Prog Neurobiol* **70**, 363-386 (2003). https://doi.org:10.1016/s0301-0082(03)00090-x

65 Zhu, S. *et al.* Nigericin treatment activates endoplasmic reticulum apoptosis pathway in goldfish kidney leukocytes. *Fish Shellfish Immunol* **134**, 108616 (2023). https://doi.org:10.1016/j.fsi.2023.108616

66 Cai, X. Unicellular Ca2+ signaling 'toolkit' at the origin of metazoa. *Mol Biol Evol* **25**, 1357-1361 (2008). https://doi.org:10.1093/molbev/msn077

67 Gandara, A. C. P., Torres, A., Bahia, A. C., Oliveira, P. L. & Schama, R. Evolutionary origin and function of NOX4-art, an arthropod specific NADPH oxidase. *BMC Evol Biol* **17**, 92 (2017). https://doi.org:10.1186/s12862-017-0940-0

68 Tompkins-Macdonald, G. J. *et al.* Expression of a poriferan potassium channel: insights into the evolution of ion channels in metazoans. *J Exp Biol* **212**, 761-767 (2009). https://doi.org:10.1242/jeb.026971

69 P.M., H. The inter-relationships of bivalve haemocytes. *Fish & Shellfish Immunology* **9**, pp.367-385. (1999).

70 Do, E. A. & Gries, C. M. Beyond Homeostasis: Potassium and Pathogenesis during Bacterial Infections. *Infect Immun* **89**, e0076620 (2021). https://doi.org:10.1128/IAI.00766-20

71 Khan, M. A. & Palaniyar, N. Transcriptional firing helps to drive NETosis. *Sci Rep* **7**, 41749 (2017). https://doi.org:10.1038/srep41749

72 Skinner, B. M. & Johnson, E. E. Nuclear morphologies: their diversity and functional relevance. *Chromosoma* **126**, 195-212 (2017). https://doi.org:10.1007/s00412-016-0614-5

73 Acharya, M. *et al.* alphav Integrins combine with LC3 and atg5 to regulate Toll-like receptor signalling in B cells. *Nat Commun* **7**, 10917 (2016). https://doi.org:10.1038/ncomms10917

732 **Figures**

Figure 1

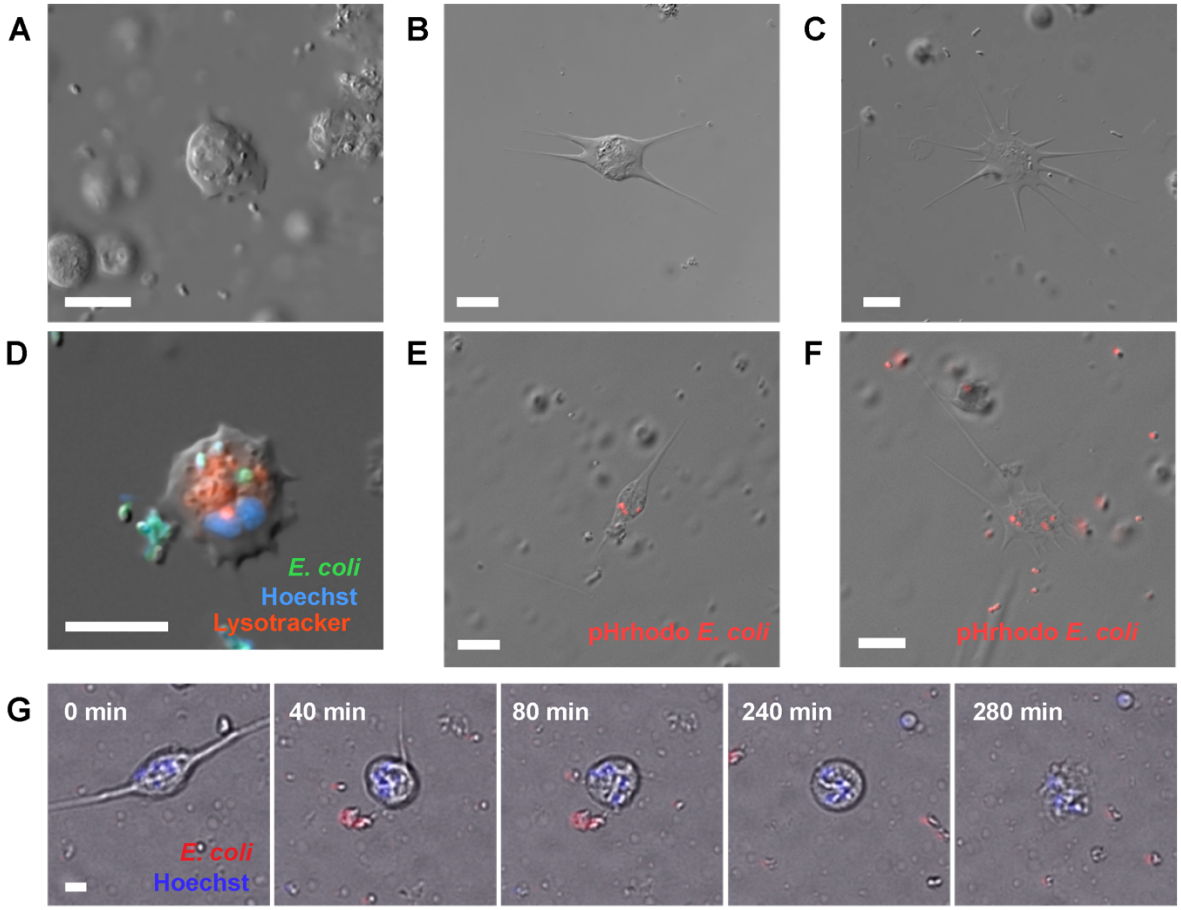

733
734

Figure 2

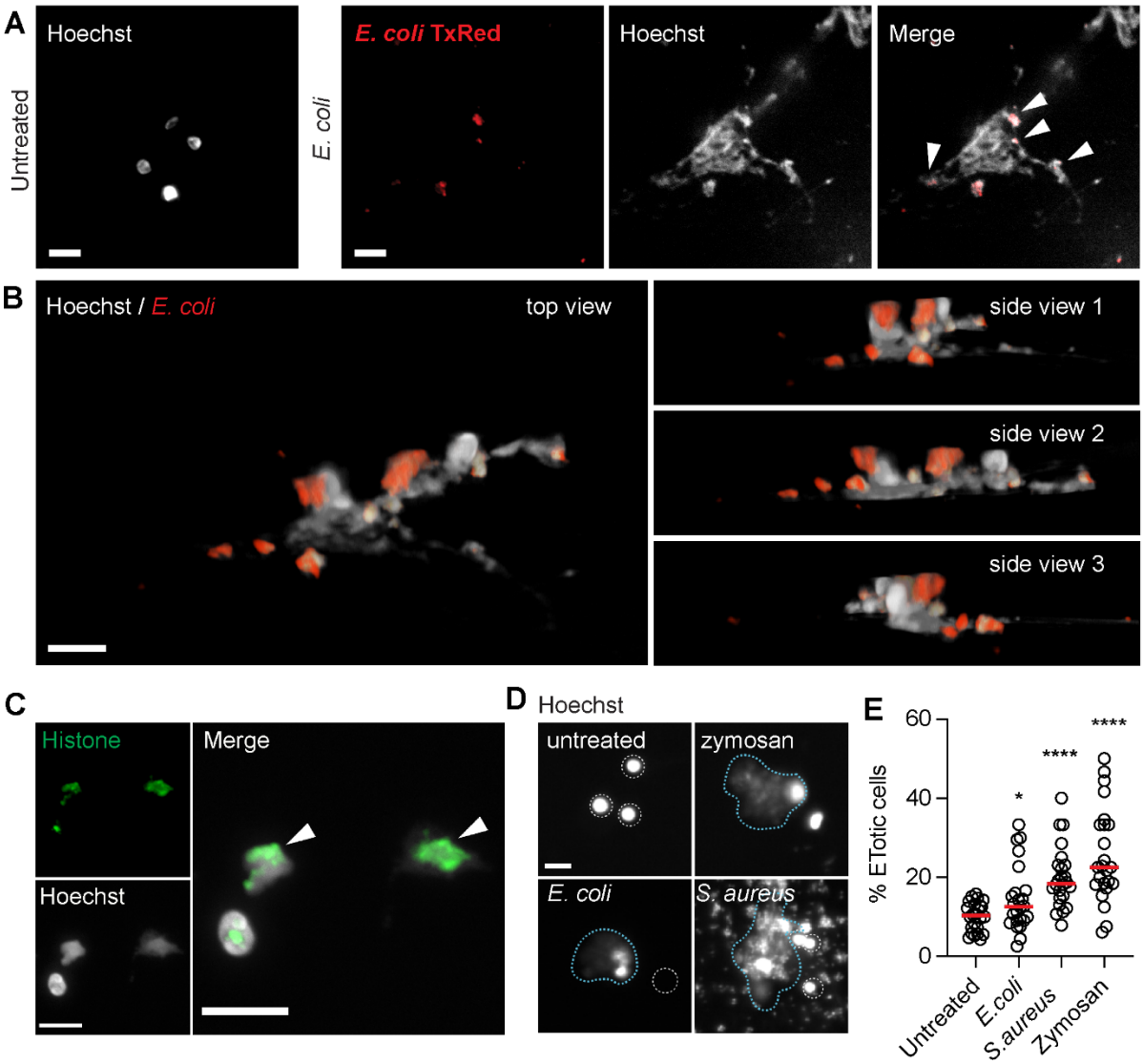
A
Untreated
Hoechst
E. coli
E. coli TxRed
Hoechst
Merge
B
Hoechst / E. coli
top view
side view 1
side view 2
side view 3
C
Histone
Merge
Hoechst
D
Hoechst
untreated
zymosan
E. coli
S. aureus
E
% ETotic cells
60
40
20
0
*
****
****
Untreated
E.coli
S.aureus
Zymosan

Figure 3

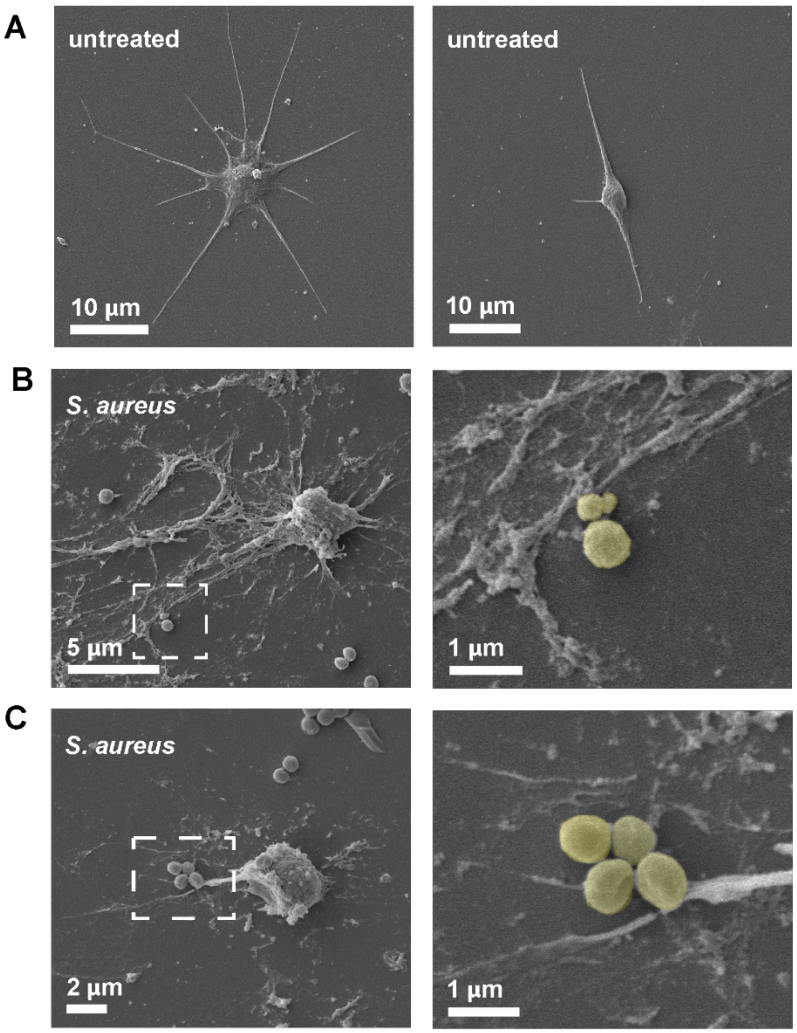

737
738

739

Figure 4

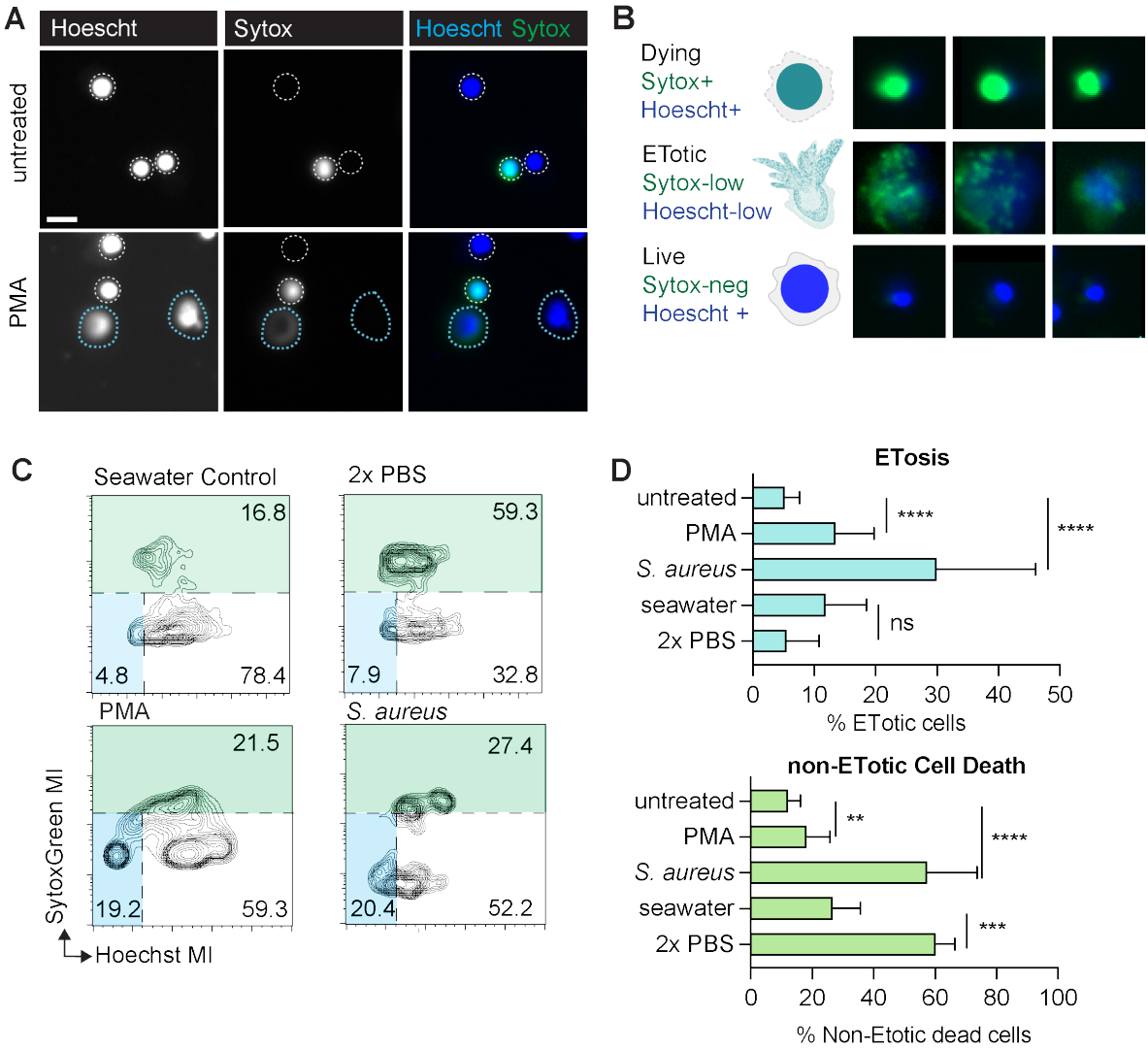
A
Hoescht
Sytox
Hoescht Sytox
untreated
PMA
B
Dying
Sytox+
Hoescht+
ETotic
Sytox-low
Hoescht-low
Live
Sytox-neg
Hoescht +
C
Seawater Control
2x PBS
PMA
S. aureus
16.8
4.8
78.4
59.3
7.9
32.8
21.5
19.2
59.3
27.4
20.4
52.2
SytoxGreen MI
Hoechst MI
D
ETosis
untreated
PMA
S. aureus
seawater
2x PBS
****
****
ns
0
10
20
30
40
50
% ETotic cells
non-ETotic Cell Death
**
****
***
0
20
40
60
80
100
% Non-Etotic dead cells

740

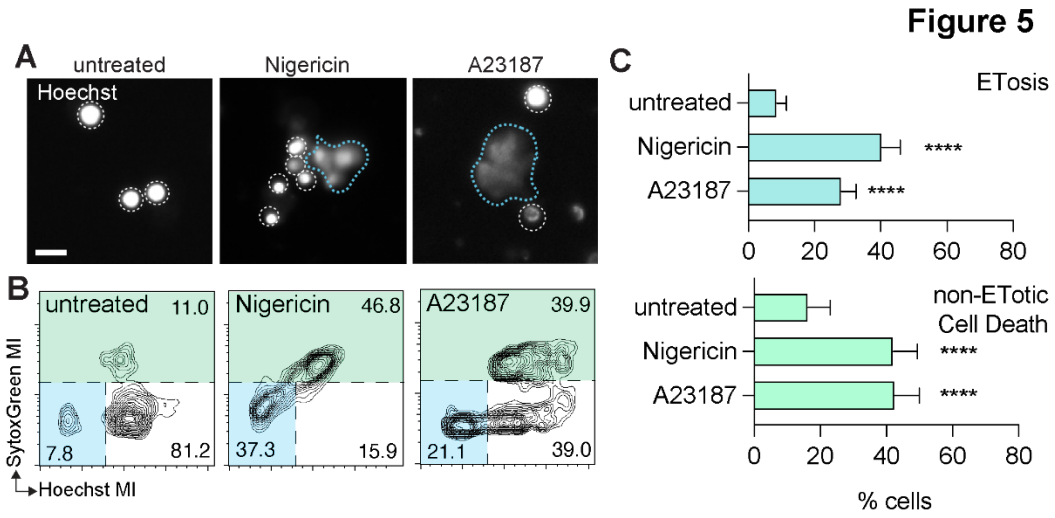
Figure 5
A
untreated
Nigericin
A23187
Hoechst
B
untreated 11.0
7.8
81.2
Nigericin 46.8
37.3
15.9
A23187 39.9
21.1
39.0
SytoxGreen MI
Hoechst MI
C
ETosis
untreated
Nigericin
A23187
****
****
0
20
40
60
80
non-ETotic
Cell Death
untreated
Nigericin
A23187
****
****
0
20
40
60
80
% cells

741
742

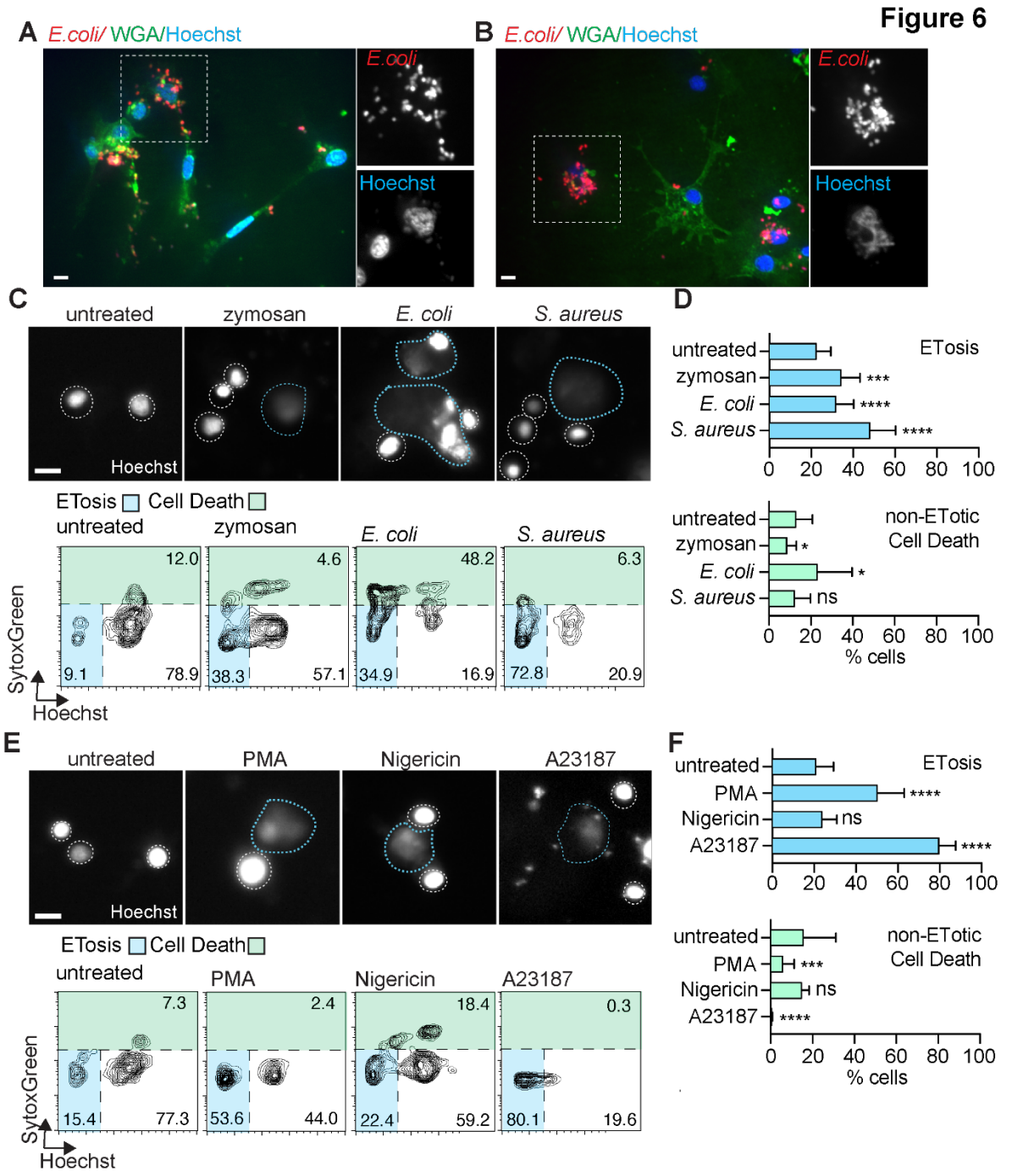
Figure 6
A
E.coli/ WGA/Hoechst
E.coli
Hoechst
B
E.coli/ WGA/Hoechst
E.coli
Hoechst
C
untreated
zymosan
E. coli
S. aureus
Hoechst
ETosis
Cell Death
untreated
zymosan
E. coli
S. aureus
12.0
4.6
48.2
6.3
9.1
78.9
38.3
57.1
34.9
16.9
72.8
20.9
SytoxGreen
Hoechst
D
ETosis
untreated
zymosan
E. coli
S. aureus
***
****
****
0
20
40
60
80
100
non-ETotic
Cell Death
untreated
zymosan
E. coli
S. aureus
*
*
ns
% cells
E
untreated
PMA
Nigericin
A23187
Hoechst
ETosis
Cell Death
untreated
PMA
Nigericin
A23187
7.3
2.4
18.4
0.3
15.4
77.3
53.6
44.0
22.4
59.2
80.1
19.6
SytoxGreen
Hoechst
F
ETosis
untreated
PMA
Nigericin
A23187
****
ns
****
0
20
40
60
80
100
non-ETotic
Cell Death
untreated
PMA
Nigericin
A23187
***
ns
****
% cells

743
744

Figure 7

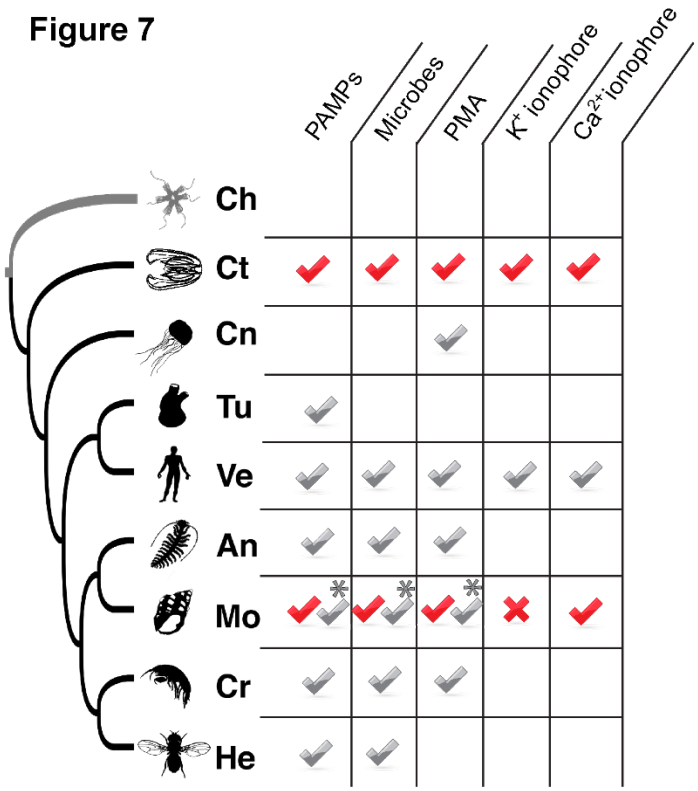
PAMPs
Microbes
PMA
K+ ionophore
Ca2+ ionophore
Ch
Ct
Cn
Tu
Ve
An
Mo
Cr
He

745